

Sensitivity analysis and parametric study of elastic properties of an unidirectional mineralized bone fibril-array using mean field methods

Andreas G. Reisinger · Dieter H. Pahr ·
Philippe K. Zysset

Received: 19 June 2009 / Accepted: 18 January 2010
© Springer-Verlag 2010

Abstract The key parameters determining the elastic properties of an unidirectional mineralized bone fibril-array decomposed in two further hierarchical levels are investigated using mean field methods. Modeling of the elastic properties of mineralized micro- and nanostructures requires accurate information about the underlying topology and the constituents' material properties. These input data are still afflicted by great uncertainties and their influence on computed elastic constants of a bone fibril-array remains unclear. In this work, mean field methods are applied to model mineralized fibrils, the extra-fibrillar matrix and the resulting fibril-array. The isotropic or transverse isotropic elastic constants of these constituents are computed as a function of degree of mineralization, mineral distribution between fibrils and extra-fibrillar matrix, collagen stiffness and fibril volume fraction. The linear sensitivity of the elastic constants was assessed at a default set of the above parameters. The strain ratios between the constituents as well as the axial and transverse indentation moduli of the fibril-array were calculated for comparison with experiments. Results indicate that the degree of mineralization and the collagen stiffness dominate fibril-array elasticity. Interestingly, the stiffness of the extra-fibrillar matrix has a strong influence on transverse and shear moduli of the fibril-array. The axial strain of the intra-fibrillar mineral platelets is 30–90% of the applied fibril strain, depending on mineralization and collagen stiffness. The fibril-to-fibril-array strain ratio is essentially ~ 1 . This study provides an improved insight in the parameters, which govern the fibril-array stiffness of mineralized tissues such as bone.

Keywords Bone · Elastic constants · Fibril array · Mean field method · Micromechanical model · Sensitivity analysis

1 Introduction

Bone is a mineralized tissue, organized along multiple length scales down to the molecular level. Regarding its mechanical function, it is comparably stiff, resistant and tough while being lightweight. In order to understand these remarkable macroscopic mechanical properties, the structure and function of the underlying levels of organization as well as their interaction have to be investigated. Above all, this knowledge is important for the assessment of bone metabolic diseases such as osteoporosis or osteogenesis imperfecta, which cause pathologic changes in bone stiffness, strength and toughness that may be partially attributed to the lower levels of organization.

Bone tissue presents a variety of microstructural motives depending on species and anatomical location that fulfill different metabolic and mechanical requirements. The bone tissue considered in this article is lamellar bone, the most common bone motive in the human body and many mammals. It is found in bone structural units called osteons for compact bone and trabecular packets for cancellous bone (Rho et al. 1998). The microstructure of lamellar bone is subdivided in the following hierarchical levels as shown in Fig. 1. Each lamella is supposed to be made of several sub-lamellae, each being formed of an unidirectionally aligned fibril-array (Weiner et al. 1997). The alignment rotates subsequently from sub-lamella to sub-lamella giving rise to a plywood-like structure in a single bone lamella (Giraud-Guille 1988; Weiner et al. 1997; Wagermaier et al. 2006). The fibril-array is an unidirectional fibrous composite made of mineralized

A. G. Reisinger (✉) · D. H. Pahr · P. K. Zysset
Vienna University of Technology, Institute of Lightweight Design and Structural Biomechanics, Gußhausstraße 27-29, 1040 Vienna, Austria
e-mail: andreas.reisinger@tuwien.ac.at

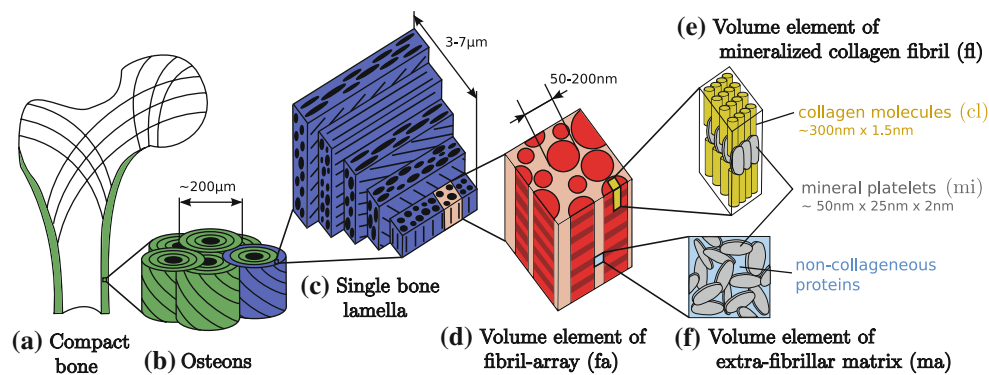


Fig. 1 Microstructure of bone: (Weiner and Wagner 1998; Weiner et al. 1999; Rho et al. 1998; Giraud-Guille 1988; Fratzl et al. 2004; Fratzl and Weinkamer 2007; Lees et al. 1994; Landis and Silver 2002) **a** Compact bone in long bone diaphysis; **b** osteons, formed by lamellae, with haversian channels; **c** bone lamella, made of subsequently rotated sub-lamellae—“twisted plywood” assembly; **d** fibril-array-long unidirectionally

aligned fibrils, bond in an extra-fibrillar matrix; **e** mineralized collagen fibril-long collagen molecules, arranged in a staggered manner, giving rise to an overlapping zone and a gap zone. In the gap zone, bone mineral platelets, mainly hydroxyapatite, grow; **f** extra-fibrillar matrix-made of non-collagenous proteins and mineral, bonds fibrils together

collagen fibrils embedded in an extra-fibrillar matrix. Fibrils contain the very basic building blocks of bone: collagen type I molecules periodically reinforced by mineral platelets, mostly made of carbonated apatite (Weiner and Wagner 1998). Whereas the fibrillar structure is quite well described, the morphology of the extra-fibrillar matrix is poorly understood. There is a general agreement that it acts as a glue layer between the fibrils. It consists of a network of non-collagenous proteins like osteopontin and sialoprotein in bone (Hansma et al. 2005; Fantner et al. 2007) and proteoglycans in tendons (Cribb and Scott 1995; Raspanti et al. 2002). This network is infiltrated with extra-fibrillar bone mineral (Lees 1979; Probst and Lees 1996; Lees et al. 1994; Sasaki et al. 2002).

Current experimental techniques in mechanical testing such as microtensile tests (Hengsberger et al. 2003), microindentation (Roessle 1927), nanoindentation (Rho et al. 1997), scanning ultrasound microscopy (Katz and Meunier 1993) or atomic force microscopy (Lees et al. 1994) are limited to specific length scales and their usage requires a high amount of effort and resources. Micromechanical modeling of bone tissue is therefore an attractive, complementary method of investigation, which was used in several publications to assess the elastic stiffness properties of bone microstructures.

Akkus (2005) used micromechanical methods to calculate the elastic stiffness of a mineralized fibril and investigated the partitioning of applied stresses in the composite. He varied mineral content as well as mineral shape and investigated the impact on the fibril properties. Yoon and Cowin (2008) estimated the elastic constants of a single osteonal lamella in a multiscale approach with different micromechanical methods taking the contained water into account. Akiva et al. (1998) calculated the stiffness of a bone lamella made of sub-lamellae using a platelet reinforced composite model. Jaeger and Fratzl (2000) and Kotha et al. (2000) introduced

a 2D model of a mineralized fibril with a staggered mineral platelet arrangement and investigated the influence of changes in geometry and mineralization. Hellmich and Ulm (2002) modeled a complete went-through in bone hierarchy from the nano- to the macroscale, using a multiscale assembly of self consistent schemes and correlated the macroscopic stiffness outcome to experimental results of different types of bone tissue. Nikolov and Raabe (2008) developed a multiscale micromechanical model that leads from the mineralized fibril level to the fibril-array level. Their fibrils are coated by mineral to account for extra-fibrillar mineralization.

In such models, the basic input parameters such as mineral volume fraction and collagen stiffness have always to be obtained from measurements, which imply a number of hypotheses and are afflicted by experimental errors. For example, on the length scale of a continuous collagen matrix, axial collagen stiffness values from below 1 GPa up to 12 GPa are reported (Cusack and Miller 1979; Sasaki and Odajima 1996; van der Rijt et al. 2006).

As such measurements are the basis for continuum models of collagen assemblies, the model input is uncertain in a wide range. Some input errors may have a severe impact on the computed tissue stiffness whereas others may not. Up to the authors knowledge, there was no comprehensive sensitivity or uncertainty study of the anisotropic elastic tissue properties done so far.

Thus the basic research question of this study is the identification of the important and less important factors determining the elastic properties of a bone fibril-array. Additionally, the strain ratios between the constituents within the fibril-array are looked for. For these purposes, the hierarchical levels of a fibril-array are modeled with current knowledge including the extra-fibrillar matrix while keeping the overall number of input parameters reasonable. Accordingly, a multiscale Mori-Tanaka type mean field model is used,

which is well suited for parameter studies as it is simple and fast in comparison with unit cell finite element models but still more advanced and accurate than simple rules of mixtures.

2 Methods

2.1 Mori-Tanaka type mean field method

On one hand, the Mori-Tanaka type mean field method is an analytical technique in continuum mechanics to estimate homogenized linear anisotropic elastic properties of composites, consisting of an inclusion-matrix topology (Mori 1973; Benveniste 1987). On the other hand, it can be used for the localization of a macroscopically applied strain- or stress state on the composite to the resulting strain- and stress fields in the underlying phases. All field quantities, such as strain and stress, are described in terms of volume averages in the corresponding phases. Inclusions are randomly distributed in space and perfectly bonded to the matrix. For all investigations in this article, unidirectionally aligned Eshelby type spheroidal inclusions were used (1957 2007; Withers 1989). More realistic inclusion shapes would require preliminary numerical investigations as they cannot be included analytically in the model.

Input parameters of a meanfield model are the elastic properties of the inclusions ${}^i\mathbf{E}$ and the matrix ${}^m\mathbf{E}$, the inclusion volume fraction φ and the inclusion aspect ratio $a = l/d$ (Fig. 2).

2.2 Multiscale homogenization

The basic workflow is the following Fig. 3: In the first homogenization step, the stiffness tensors of a mineralized collagen fibril and the extra-fibrillar matrix are calculated. In a second homogenization step, the previously obtained elastic properties are substituted into the fibril-array model to finally obtain the fibril-array stiffness.

Mineralized fibril:

Mineralized fibrillar structure is modeled as a continuous isotropic collagen matrix with enclosed isotropic mineral

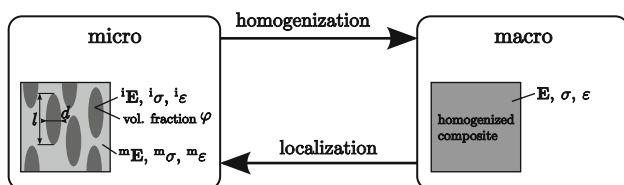


Fig. 2 Mean field method: A composite material is made of spheroidal inclusions (i) which are bound in a matrix (m) (left). The homogenized stiffness tensor \mathbf{E} (right) as well as the relationship between the localized stresses and strains ${}^i\sigma$, ${}^i\epsilon$, ${}^m\sigma$, ${}^m\epsilon$ and the macroscopic stresses and strains σ , ϵ is predictable

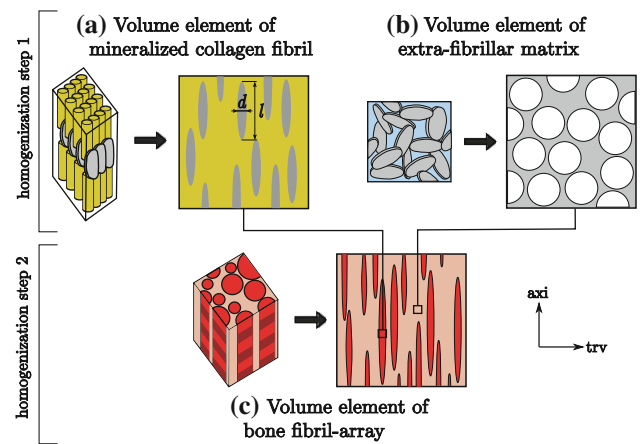


Fig. 3 Mean field model representations of bone micro- and nanostructures and multiscale workflow: **a** fibril structure is modeled as a composite with prolate isotropic mineral spheroids unidirectionally embedded in an isotropic collagen matrix; **b** extra-fibrillar mineral-protein network is modeled as a mineral foam with spherical voids; **c** fibril-array is built of highly elongated prolate spheroids of fibril material, embedded in extra-fibrillar matrix material

spheroids (Fig. 3a). They are unidirectionally aligned but randomly distributed in space. They do not represent neither the exact shape nor the staggered arrangement of the mineral platelets in the fibril. The resulting stiffness tensor is therefore transverse isotropic and not orthotropic.

Extra-fibrillar matrix:

There is widespread agreement that the extra-fibrillar matrix acts as a glue, in which fibrils are bonded by a network of non-collagenous molecules, such as osteopontin (Fantner et al. 2007). This network is supposed to be interpenetrated by bone mineral. Lees et al. (1994) found evidence for a high mineral content in the extra-fibrillar matrix in mineralized turkey leg tendon and (Prostak and Lees 1996) in human bone. Gupta et al. (2005) proposed a shear compliant mineralized extra-fibrillar matrix. Our model assumes that the stiffness of the extra-fibrillar matrix is mainly influenced by the embedded mineral. The comparatively thin and soft protein network is disregarded. The extra-fibrillar matrix is therefore modeled as a porous mineral network with spherical voids (Fig. 3b), in contrast to the view of Gupta et al. (2005).

Fibril-array:

The length of a mineralized fibril is barely reported in the literature. Silver et al. (2003) observed continuing selfassembly of nascent fibril segments to long fibrils of more than $106\text{ }\mu\text{m}$. Birk et al. (1997) did a 3D reconstruction of a few fibrils in chicken tendon, not observing both ends of a fibril in his $60\text{ }\mu\text{m}$ long observation window. The fibrils are obviously very long compared to their diameter. Hence the fibril-array is most likely a *long* fiber composite in which the aspect ratio of the inclusions is very high to infinite. All aspect ratios above a certain value lead to the same composite elastic

properties. In our model, this is accounted for by setting the aspect ratio of the fibril inclusions to a very high value of $^{fa}a = l/d = 100$. The fibril inclusions are embedded unidirectionally and randomly distributed in space in a continuous extra-fibrillar matrix (Fig. 3c).

2.3 Mineral distribution parameter

The ratio between fibril- and extra-fibrillar matrix mineralization is treated as an indeterminate parameter in this study, although there are a few publications addressing this issue. [Lees et al. \(1994\)](#) reported 25–30% of the mineral in mineralized turkey leg tendon fibers to be in the fibrils and 70–75% to be in the extra-fibrillar matrix, as seen in TEM pictures. [Sasaki et al. \(2002\)](#) proposed a ratio of 23/77% based on volume distribution estimations in bovine bone. These values are not obtained from lamellar bone and therefore possibly not suitable for our investigations. So we introduce a dimensionless mineral distribution parameter $^{fl}\alpha$, which determines the fraction of the fibril-array mineral to be situated in the fibril and $^{ma}\alpha = 1 - ^{fl}\alpha$ the fraction in the extra-fibrillar matrix. The actual mineral volume fractions in the fibril $^{mi,fl}\varphi$ and in the extra-fibrillar matrix $^{mi,ma}\varphi$ are then given by

$$^{mi,fl}\varphi = ^{fl}\alpha \frac{^{mi,fa}\varphi}{^{fl,fa}\varphi} \quad ^{mi,ma}\varphi = (1 - ^{fl}\alpha) \frac{^{mi,fa}\varphi}{1 - ^{fl,fa}\varphi} \quad (1)$$

Where $^{mi,fa}\varphi$ is the mineral volume fraction in the fibril-array and $^{fl,fa}\varphi$ the volume fraction of the fibrils in the fibril-array. The variable φ generally denotes volume fractions. Phase abbreviations are shown in Fig. 1.

2.4 Set of input parameters

In Table 1, the full set of input parameters is shown. From our point of view, the most uncertain parameters in our model of bone microstructure are collagen stiffness ^{cl}E , the fibril volume fraction in the fibril-array $^{fl,fa}\varphi$ and the mineral distribution between fibrils and extra-fibrillar matrix $^{fl}\alpha$. The mineral volume fraction in the fibril-array $^{mi,fa}\varphi$ is variable and can be determined by experiments. The above four parameters are varied in a broad range to investigate their impact on the microstructural stiffness closely. All other parameters are fixed to meaningful *operation point* values from the literature to keep the number of free parameters small. Also the four uncertain quantities have an operation point since only two parameters are varied at the same time.

For collagen stiffness ^{cl}E , a wide range of values on different length scales are reported in literature. In this work, collagen is considered as a continuous collagen matrix. Its elastic properties should match the characteristics of a representative volume element of an unmineralized collagen fibril, in which a sufficient number of collagen molecules and crosslinks are included. Such elastic properties were measured experimentally by [Cusack and Miller \(1979\)](#), [Sasaki and Odajima \(1996\)](#), [van der Rijt et al. \(2006\)](#) who report axial Young's moduli between below 1 GPa up to 12 GPa dependent on the applied technique and the water content of the sample. Accounting for this wide distribution, the Young's modulus of collagen is varied between 1 and 9 GPa in the model. The operation point value is $^{cl}E_0 = 5$ GPa, which corresponds to wet collagen in ([Cusack and Miller 1979](#)) and interestingly at the same time to dry collagen in

Table 1 List of model input parameters (left part) and linear sensitivity of fibril-array stiffness (right part): operation point values are supposed to represent the configuration of an average lamellar bone sample

Input parameter	Variable	Operation point	Unit	Literature	Variation range	Sensitivity of $^{fa}E_{axi}$ in GPa	Sensitivity of $^{fa}E_{axi}/^{fa}E_{trv}$
Collagen Young's modulus	^{cl}E	$^{cl}E_0 = 5$	GPa	(van der Rijt et al. 2006)	1–9	± 0.81	∓ 0.071
Collagen Poisson ratio	$^{cl}\nu$	$^{cl}\nu_0 = 0.3$	1	–	–	∓ 0.37	∓ 0.44
Mineral Young's modulus	^{mi}E	$^{mi}E_0 = 110.15$	GPa	(Yao et al. 2007)	–	± 0.18	± 0.0032
Mineral Poisson ratio	$^{mi}\nu$	$^{mi}\nu_0 = 0.28$	1	(Yao et al. 2007)	–	∓ 0.036	∓ 0.056
Mineral platelet aspect ratio in fibril	^{fl}a	$^{fl}a_0 = 14$	1	(Akkus 2005)	–	± 0.19	± 0.012
Void aspect ratio in extra-fibrillar matrix	^{ma}a	$^{ma}a_0 = 1$	1	–	–	–	–
Fibril aspect ratio in fibril-array	^{fa}a	$^{fa}a_0 = 100$	1	(Birk et al. 1997)	–	± 0.0001	~ 0
Fibril volume fraction in fibril-array	$^{fl,fa}\varphi$	$^{fl,fa}\varphi_0 = 0.5$	1	(Fritsch and Hellmich 2007)	0.2–0.8	± 13.82	± 1.17
Mineral volume fraction in fibril-array	$^{mi,fa}\varphi$	$^{mi,fa}\varphi_0 = 0.3$	1	(Currey 2004)	0.15–0.45	± 87.7	± 1.23
Mineral distribution parameter	$^{fl}\alpha$	$^{fl}\alpha_0 = 0.25$	1	(Lees et al. 1994) (Sasaki et al. 2002)	0–1	∓ 4.8	± 0.68

They define the model's default state in which the linear sensitivity of the fibril-array elastic properties $^{fa}E_{axi}$ and $^{fa}E_{axi}/^{fa}E_{trv}$ is computed. The sensitivity values indicate the change of the particular fibril-array property for a variation of the respective input parameter of ± 1 , assuming linear behavior. The influences of ^{cl}E , $^{fl,fa}\varphi$, $^{mi,fa}\varphi$ and $^{fl}\alpha$ are studied in more detail in Figs. 4, 5, 7, 6 and 8 and are therefore varied in given specific ranges

(van der Rijt et al. 2006). The Poisson ratio is assumed and fixed to ${}^{\text{cl}}\nu = 0.3$.

Mineral platelets in bone have dimensions in the nanometer scale, their structure can be regarded as perfectly crystalline and defect free (Su et al. 2003). Mineral elastic properties are therefore taken from *ab initio* calculations of hydroxyapatite stiffness (Yao et al. 2007).

The mineral inclusions aspect ratio of ${}^{\text{fl}}a = 40/3 \approx 14$ was derived by Akkus (2005) from geometrical considerations of the available space in a collagen fibril. Mineral platelets, growing in the gap region of a collagen fibril, compress the collagenous matrix in transverse direction, reaching a width of $\sim 3\text{nm}$, and fully occupy the gap length of 40nm . Reported mineral dimensions (Weiner and Traub 1992; Landis and Silver 2002; Eppell et al. 2001) are scattered in a wide range around the proposed aspect ratio. Nevertheless, it is not chosen as a free parameter because its influence on fibril stiffness was already investigated in Akkus 2005.

The volume fraction of fibrils in the fibril-array ${}^{\text{fl},\text{fa}}\varphi$ is varied in a range of 0.2–0.8. The upper bound 0.8 represents densely packed fibrils with 2 nm spacing between neighbors (Gupta et al. 2006). In addition, the bandwidth is consistent with estimates for a wide range of mineralized tissues (Hellmich et al. 2004; Fritsch and Hellmich 2007; Fritsch et al. 2009) which were based on the “Generalized Packing Model” of Lees (1987). The operation point value of ${}^{\text{fl},\text{fa}}\varphi_0 = 0.5$ meets the proposed values for human bone. As the model of Lees contains assumptions and its fibril volume fraction estimates were, to our knowledge, not validated by experiments, we consider ${}^{\text{fl},\text{fa}}\varphi$ as a parameter that needs closer investigation.

The degree of fibril-array mineralization ${}^{\text{mi},\text{fa}}\varphi$ is varied between 0.15 and 0.45 mineral volume fraction. A range including deer antler, mineralized turkey leg tendon and human bone. The operation point is set to a mean degree of mineralization that occurs in human lamellar bone, ${}^{\text{mi},\text{fa}}\varphi_0 = 0.3$ (Currey 2004).

The mineral distribution parameter variation includes both extremes. For ${}^{\text{fl}}\alpha = 0$, the whole fibril-array mineral available is situated in the extra-fibrillar matrix and for ${}^{\text{fl}}\alpha = 1$ it is situated in the fibrils only. The operation point value of 0.25 is a rough estimation from (Lees et al. 1994), and (Sasaki et al. 2002).

3 Results

3.1 Fibril-array stiffness sensitivity at the operation point

The linear sensitivity of the axial fibril-array stiffness ${}^{\text{fa}}E_{\text{axi}}$ and the degree of anisotropy, which is the ratio of axial and transverse stiffness ${}^{\text{fa}}E_{\text{axi}}/{}^{\text{fa}}E_{\text{trv}}$, on every input parameter in Table 1 is calculated. The model configuration to which

the obtained sensitivity values belong to, is called the operation point whose respective state variables are denoted with a 0-subscript. For example, the linear sensitivity of ${}^{\text{fa}}E_{\text{axi}}$ on the fibril-array mineralization ${}^{\text{mi},\text{fa}}\varphi$ at the operation point is given by

$$\left. \frac{\partial {}^{\text{fa}}E_{\text{axi}}}{\partial {}^{\text{mi},\text{fa}}\varphi} \right|_0 \quad (2)$$

For a variation of an input parameter by the extent of ± 1 , the resulting change in the fibril-array properties for linearized behavior is listed in the right two columns of Table 1. These values have to be interpreted with respect to the magnitude of the input parameter. For instance, a shift of 1 GPa in the collagen Young’s modulus may be a severe modification of the model configuration, whereas the same shift in the mineral Young’s modulus is negligible.

In this context, the fibril-array mineralization ${}^{\text{mi},\text{fa}}\varphi$ is identified as the most crucial for tissue stiffness by adding 8.8 GPa to ${}^{\text{fa}}E_{\text{axi}}$ and 0.12 to ${}^{\text{fa}}E_{\text{axi}}/{}^{\text{fa}}E_{\text{trv}}$ for a raise of 0.1. The fibril volume fraction in the fibril-array ${}^{\text{fl},\text{fa}}\varphi$ is the second sensitive parameter. It adds 1.4 GPa to ${}^{\text{fa}}E_{\text{axi}}$ and 0.12 to ${}^{\text{fa}}E_{\text{axi}}/{}^{\text{fa}}E_{\text{trv}}$ for a raise of 0.1. The constituents Poisson ratios ${}^{\text{cl}}\nu, {}^{\text{mi}}\nu$ as well as the fibril aspect ratio ${}^{\text{fa}}a$ have globally only little impact. The rest of the input parameters cause moderate changes depending on their own typical variations around the operation point.

The model behavior is non-linear with respect to most input parameters. So the presented values in Table 1 describe only punctual sensitivities that might change when the model state is not at the operation point.

3.2 Fibril and extra-fibrillar matrix elastic constants

The results of the first homogenization step according to Fig. 3 are the elastic constants of fibril tissue and extra-fibrillar matrix. As a parameter study in four parameters cannot be depicted in one graph, the study is split into two two-dimensional investigations.

In Fig. 4, the mineral distribution parameter ${}^{\text{fl}}\alpha$ and the volume fraction of fibrils in the fibril-array ${}^{\text{fl},\text{fa}}\varphi$ are varied, while all other parameters are kept constant at their operation point values listed in Table 1.

The fibril possesses transverse isotropic behavior. The extra-fibrillar matrix is isotropic due to its spherical voids and isotropic material input (Tandon and Weng 1984). For increasing ${}^{\text{fl}}\alpha$ and decreasing ${}^{\text{fl},\text{fa}}\varphi$, the fibril stiffness generally increases because its mineral content ${}^{\text{mi},\text{fl}}\varphi$ according to Eq. 1 grows. The axial direction is primarily affected due to the alignment of the elongated mineral particles. At the same time, the extra-fibrillar matrix stiffness decreases. The Poisson ratios of both modeled materials remain fairly

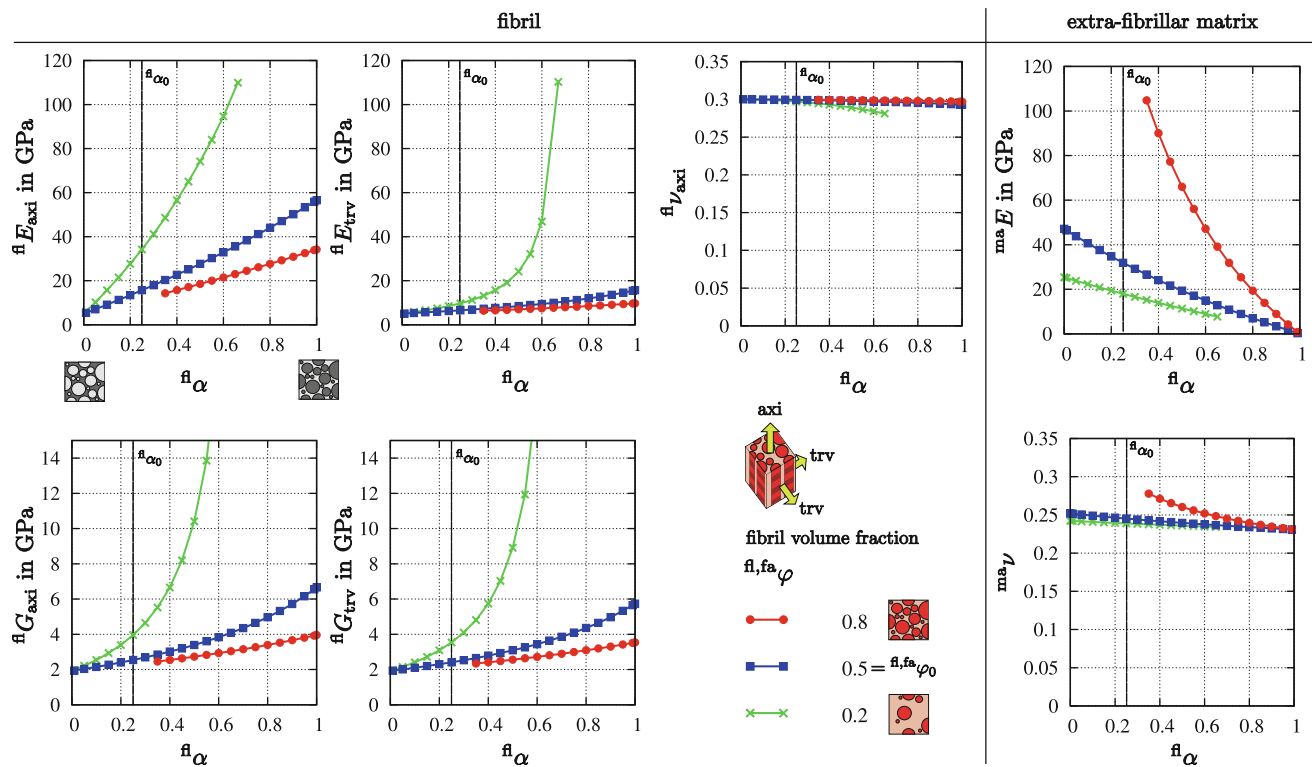


Fig. 4 Resulting elastic constants of fibril (*left*) and extra-fibrillar matrix material (*right*), depending on the mineral distribution parameter f_α and the fibril volume fraction in the fibril-array $f_{fa}\varphi$. The remaining

input parameters were left at operation point values, $mi_{fa}\varphi = 0.3$ and $clE = 5$ GPa. The axial Poisson ratio is defined as the ratio of transverse to axial strain

constant. $f_\alpha \rightarrow 1$ results in $maE \rightarrow 0$ as the whole extra-fibrillar matrix material vanishes in the model.

For the very sparse fibril array $f_{fa}\varphi = 0.2$, the fibril mineral content $mi_{f}\varphi$ reaches 100% at $f_\alpha = 0.67$. Same for the matrix at $f_{fa}\varphi = 0.8$ and $f_\alpha = 0.28$. The respective lines in the graphs stop at this points. Generally, the physical meaning of results with inclusion volume fractions above 90% is questionable.

In Fig. 5, f_α and $f_{fa}\varphi$ are now set to operation point values and the collagen Young's modulus clE and the fibril-array mineralization $mi_{fa}\varphi$ are varied. Generally, the fibrils are less stiff than the extra-fibrillar matrix because the main portion of the mineral is located in the matrix. For a variation of 1–9 GPa in collagen stiffness, the fibril stiffness shows a change of more than 100% in axial and nearly one order of magnitude in transverse direction. The impact decreases with increasing clE . Fibril-array mineralization $mi_{fa}\varphi$ strongly influences axial and transverse stiffness of both structures. Poisson ratios keep fairly constant for either parameter variation.

3.3 Fibril-array elastic constants

Elastic constants of fibril and extra-fibrillar matrix are now used to determine the fibril-array elastic constants in the

second homogenization step, as depicted in Fig. 3. In (Fig. 6) it can be seen that the impact of f_α has lost its strength when looking on fibril-array axial stiffness faE_{axi} . The reason is the opposing trend in fibril- and extra-fibrillar matrix stiffness, which neutralize each other in this homogenization step. This also dampens the effect of the fibril volume fraction variation severely in every elastic constant characteristic. The fibril-array loses stiffness in transverse direction and shear for increasing f_α , which corresponds to a softening of the extra-fibrillar matrix due to its decrease in mineral content. At the same time fibrils become more rigid but they cannot compensate this weakening tendency. For f_α close to 1, the cohesion of the composite in transverse direction and shear is decreasing rapidly.

While f_α and $f_{fa}\varphi$ have less impact on overall tissue properties in this homogenization step, collagen stiffness clE and the volume fraction of mineral in the fibril-array $mi_{fa}\varphi$ strongly influence fibril-array stiffness (Fig. 7). In fact, there are similar tendencies as in the fibril properties study in Fig. 5. For a fixed degree of mineralization, the variation in $clE = 1 - 9$ GPa causes axial and transverse Young's moduli and shear moduli to change significantly. For a fibril volume fraction higher than the chosen $f_{fa}\varphi = 0.5$, this impact would even increase.

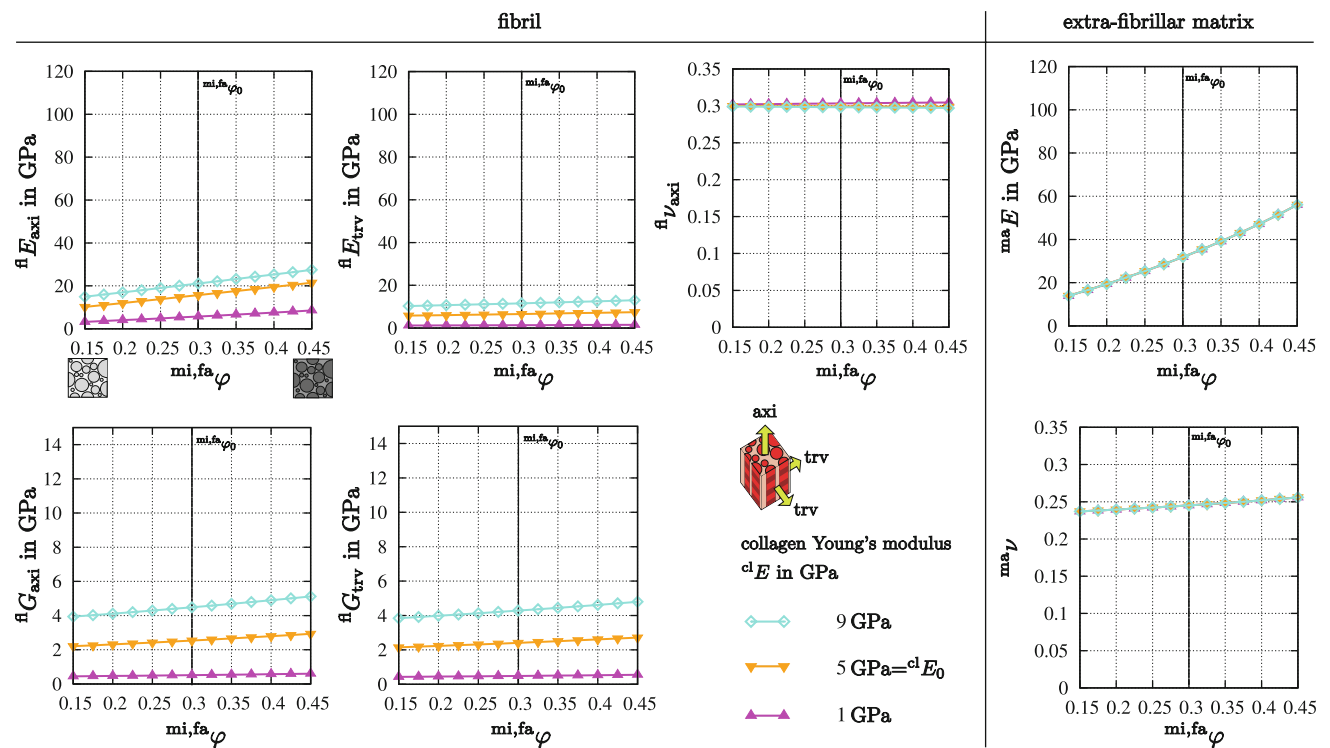
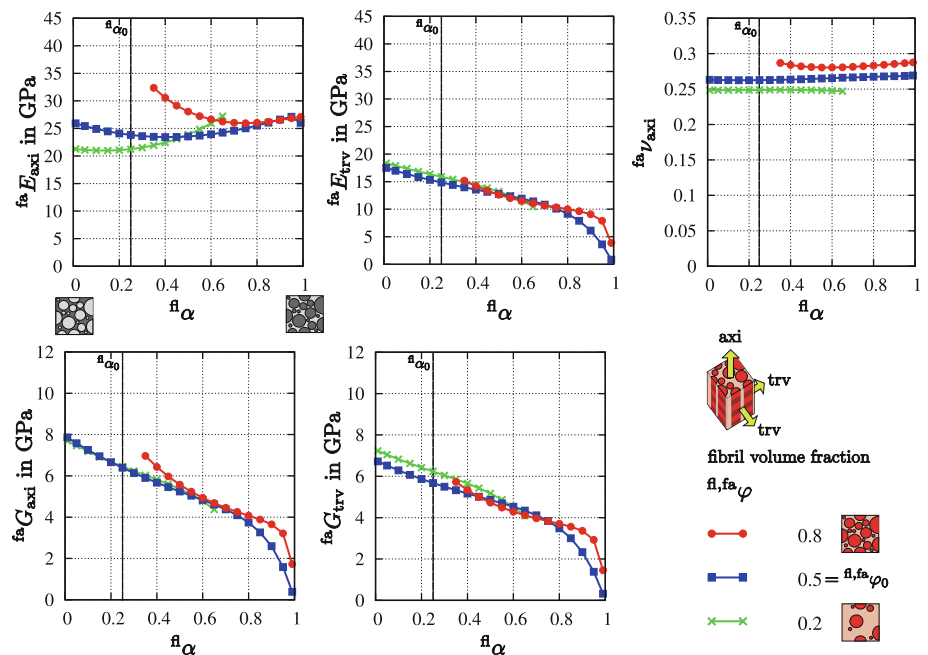


Fig. 5 Resulting elastic constants of fibril (*left*) and extra-fibrillar matrix material (*right*), depending on the volume fraction of mineral in the fibril-array $mi,fa\varphi$ and the collagen stiffness clE . The remaining

input parameters were left at operation point values, $fl,fa\varphi = 0.5$ and $fl\alpha = 0.25$. The axial Poisson ratio is defined as the ratio of transverse to axial strain

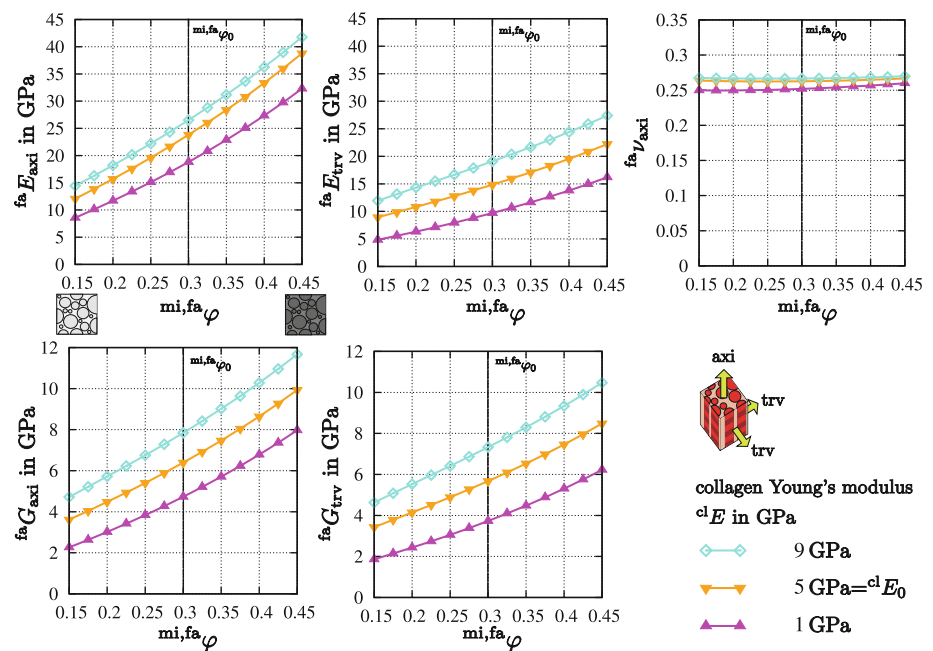
Fig. 6 Resulting elastic constants of the fibril-array, depending on the mineral distribution parameter $fl\alpha$ and the fibril volume fraction in the fibril-array $fl,fa\varphi$. The remaining input parameters were left at operation point values, $mi,fa\varphi = 0.3$ and $clE = 5$ GPa. The axial Poisson ratio is defined as the ratio of transverse to axial strain



The variation in fibril-array mineralization $mi,fa\varphi$ affects all stiffness constants severely as mineral is situated in both phases. Because of this high sensitivity, the absolute elastic

constant results in Fig. 6 depend strongly on the operation point values of clE and $mi,fa\varphi$. Poisson ratio keeps constant for either parameter variation.

Fig. 7 Resulting elastic constants of the fibril-array, depending on the volume fraction of mineral in the fibril-array $mi, fa\varphi$ and the collagen stiffness clE . The remaining input parameters were left at operation point values, $fl, fa\varphi = 0.5$ and $fl\alpha = 0.25$. The axial Poisson ratio is defined as the ratio of transverse to axial strain



3.4 Multiscale strain ratios

When applying an average strain state on a fibril-array volume element, the underlying structures will experience this strain to different degrees. The mean field method relates the macroscopic strain state of a composite to the inclusion- and matrix strain state in the linear elastic range. This is used for the following results.

Axial mineral-to-fibril strain ratio:

The axial strain transition in the fibril can be described by the ratio between the axial mineral platelet strain and the fibril strain $mi, fl\epsilon_{axi}/fl\epsilon_{axi}$ (Fig. 8c). The more mineral is located in the fibril which is determined by $fl\alpha$, $fl, fa\varphi$ and $mi, fa\varphi$, the more the mineral strain approaches the fibril strain (Fig. 8a, b). When collagen becomes stiffer, properties of the composite's matrix gets closer to its inclusion properties. This results also in a higher $mi, fl\epsilon_{axi}/fl\epsilon_{axi}$ -ratio. By the variation of the four free parameters in the given ranges, mineral-to-fibril strain ratios between 0.3 and 1 can be achieved.

Axial fibril-to-fibril-array strain ratio:

The axial strain transition in the fibril-array is the ratio between axial fibril strain and fibril-array strain $fl\epsilon_{axi}/fa\epsilon_{axi}$. In the presented model, this value yields

$$\frac{fl\epsilon_{axi}}{fa\epsilon_{axi}} \approx 1 \quad (3)$$

for all parameter variations in $fl\alpha$, $fl, fa\varphi$, clE , $mi, fa\varphi$ in the ranges given in Table 1, while the others are set to operation point values. The fibrils experience almost the same strain as the fibril-array when the composite is loaded in axial direction. This is due to the highly elongated shape of the fibrils,

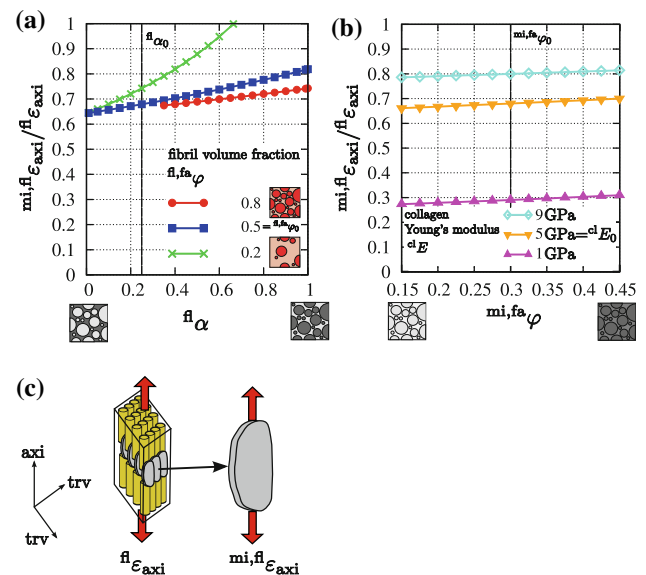


Fig. 8 Strain ratio between mineral platelet- and fibril strain: $c\ fl\epsilon_{axi}$ is the axial strain, applied on a fibril volume element and $mi, fl\epsilon_{axi}$ is the resulting strain a mineral inclusion "feels". $mi, fl\epsilon_{axi}/fl\epsilon_{axi}$ is plotted depending on the input parameters $fl\alpha$, $fl, fa\varphi$ in **a** and clE and $mi, fa\varphi$ in **b**. The not varied input parameters are set to operation point values defined in Table 1

which cause them and the extra-fibrillar matrix to deform uniformly.

4 Discussion

The multiscale micromechanical model employed in this study provides on one hand a stiffness estimation of a mineralized fibril, the extra-fibrillar matrix and a bone fibril-array

and on the other hand a basis for identifying the stiffness determinants.

As it was already proposed in many publications such as Currey (1969), Hellmich and Ulm (2002), Akkus (2005), Nikolov and Raabe (2008), we show that the mineral content of bone determines the tissue stiffness to a great extent. The variation in the literature regarding collagen stiffness, that partly arise from measurements in different conditions (wet, dry, embedded,...) also severely influences the fibril-array stiffness in the model (Fig. 7). Wet collagen, which is softer than dry collagen (Cusack and Miller 1979; van der Rijt et al. 2006), cause a softer tissue behavior on the fibril-array level. This correlation was experimentally observed on the lamella level by Hengsberger et al. (2002) who did nanoindentation measurements in cortical bone under dry and physiological conditions.

This result is an encouragement for future publications on experimentally obtained mechanical properties of bone to enclose also comprehensive compositional data of their specimens as they are important influencing variables of the results. As shown in this study, especially mineral content, specimen condition and preparation procedures are of interest.

Extra-fibrillar matrix stiffness is an influencing factor of fibril-array stiffness in transverse direction and shear, which is determined by its relative mineral content as shown in Fig. 6. This relation was also comprehensively shown by Nikolov and Raabe (2008), who used a different modeling approach than this work. They modeled the extra-fibrillar mineral as a coating around each fibril and introduced a non-collagenous protein matrix material for which they used assumed elastic properties.

In several other publications such as Hellmich and Ulm (2002), Hellmich et al. (2004), Fritsch and Hellmich (2007) the extra-fibrillar matrix was modeled via a self-consistent scheme, consisting of mineral and water. The self-consistent scheme is widely used for describing polycrystals. In the current study, the impact of the choice of the micromechanical approach for the extra-fibrillar matrix material was additionally tested by using a generalized porous self-consistent scheme instead of the default Mori-Tanaka method. The phase properties of the mineral and the pores remained unchanged. At the operation point, the extra-fibrillar matrix was found to be 13% softer, causing a slight softening of the fibril-array. The general tendencies and sensitivities of all elastic constants of all structures remain nearly unchanged, regardless which micromechanical approach was used for the extra-fibrillar matrix.

Interestingly, neither the location of the tissue mineral nor the relative amount of fibrils seem to have a remarkable effect on the stiffness output in the axial direction (Fig. 6). This results to a certain extent from the quite similar properties of the fibril and the extra-fibrillar matrix models. Variations

in the two parameters change the properties of the two models in the manner that the changes are canceled out in the fibril-array model. Regarding the location of the tissue mineral, a similar effect was also shown by Nikolov and Raabe (2008).

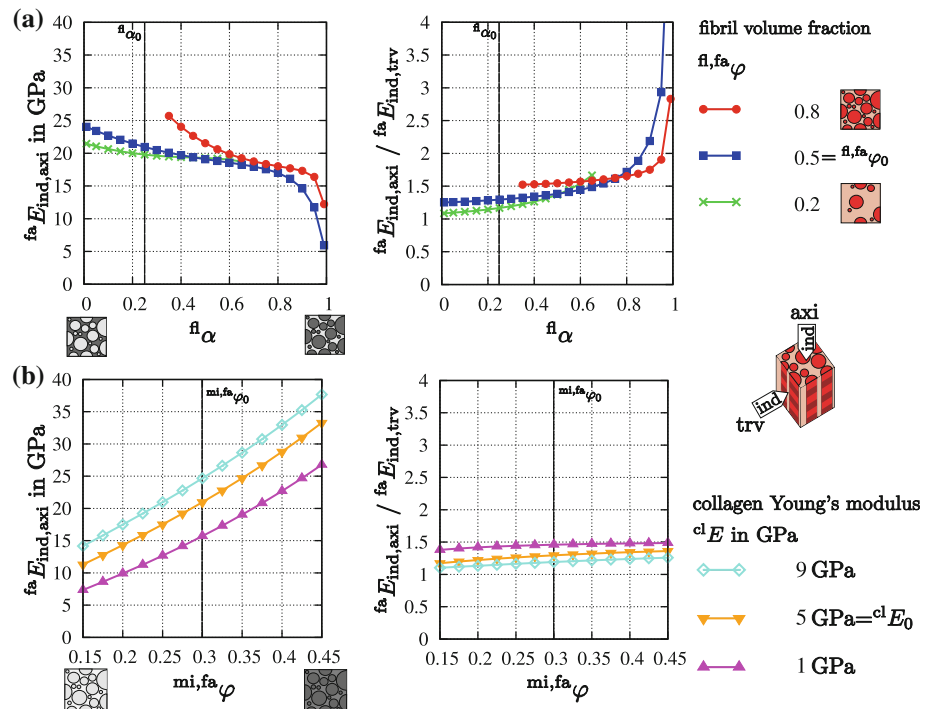
As shown in Table 1, the fibril-array axial Young's modulus and its degree of anisotropy are hardly affected by the constituents' Poisson ratios. This is due to the uniform transverse deformation of mineral and collagen as both have similar Poisson ratios at the operation point. For greater differences, the deformation mismatch of the phases transverse to the loading direction leads to a slight stiffening of the composite. Moreover, moderate variations of the mineral Young's modulus show also little impact on the stiffness indicators. For a higher overall mineralization $^{mi,fa}\varphi$ this contribution would increase.

For a variation of ± 1 in the mineral platelet aspect ratio ^{fl}a in the fibril, $^{fa}E_{axi}$ changes moderately by ± 0.19 GPa. Akkus (2005) showed that this influence decreases even more for a growth of ^{fl}a .

Interestingly, an increase in the amount of fibrils stiffens the fibril-array, even though the fibrils are less stiff than the extra-fibrillar matrix at the operation point. $^{fa}E_{axi}$ rises 1.4 GPa for a change of $+0.1$ in $^{fl,fa}\varphi$. The reason is the disproportionately high increase in extra-fibrillar matrix stiffness, that overcompensates the loss of extra-fibrillar matrix volume (Fig. 4).

At the bone lamella length scale, the currently most prominent experimental method for measuring tissue mechanical properties is nanoindentation (Ebenstein and Pruitt 2006). To offer a direct possibility of comparing the sensitivity results of this study with nanoindentation measurements, the elastic constant characteristics of Figs. 6 and 7 are transformed to longitudinal and transverse indentation moduli $^{fa}E_{ind,axi}$ and $^{fa}E_{ind,trv}$, respectively, using the theory of Swadener and Pharr (2001). See Fig. 9. In Hofmann et al. (2006), and Zysset et al. (1999), nanoindentation on whole bone-lamellae were performed. The indenter tip was too large to obtain measurements of a single sub-lamella layer which would consist of an unidirectional fibril-array structure. Their presented indentation moduli can rather be seen as combined properties of a stack of several rotated fibril-array layers that were simultaneously hit by the indenter tip. Nevertheless, their results may be used as an estimation for the magnitude of fibril-array Young's moduli. In Hofmann et al. (2006), indentation moduli between 21.2 and 26.6 GPa and in Zysset et al. (1999) values between 15.8 and 21.2 GPa were presented. In Fig. 9b, it can be seen that the output of the micromechanical model is perfectly located in the experimental result ranges for the model parameters being set to operation point values. At the same time it is shown that the same well fitting model results can be achieved by other possible and reasonable combinations of input parameters.

Fig. 9 Fibril-array indentation moduli: the axial indentation modulus $^{fa}E_{ind,axi}$ and the ratio between axial and transverse indentation moduli $^{fa}E_{ind,axi}/^{fa}E_{ind,trv}$ are computed from the elastic constant results of Figs. 6 and 7, using the theory of Swadener and Pharr (2001)



The two-scale micromechanical model will provide meaningful overall elastic properties of the tissue for many combinations of the input parameters. Parameters with a low impact can be set independently to any values without changing the results. It is therefore not possible to deduce the correctness of the input from the accordance of model outcomes with experimental outcomes. Additionally, this potential agreement does not mean that the chosen modeling approach represents the actual mechanical processes in the real tissue.

Gupta et al. (2006) investigated the strain ratios in young bovine bone tissue between the axial strains of an unidirectional fibril-array, a single fibril and the enclosed mineral platelets. For the mineral to fibril strain ratio values of $^{mi, fl} \varepsilon_{axi} / ^{fl} \varepsilon_{axi} = 0.34 \pm 0.15$ for wet and 0.53 ± 0.0 for dry tissue were reported, unfortunately without information about specimen mineralization and fibril orientation distribution. In Fig. 8b, the mineral to fibril strain ratio is represented. For soft collagen near 1 GPa, which is supposed to match the wet conditions, the model gives well fitting strain ratios around 0.3. For stiffer dry collagen, the strain ratio rises. At $^{cl} E = 2$ GPa, strain ratios between 0.43 and 0.47 are obtained, depending on tissue mineralization. The model seems therefore to be capable of describing the general elastic deformation mechanisms at the fibrillar hierarchical level. At the overlying hierarchical level, Gupta et al. (2006) reported fibril to tissue strain ratios of 0.41 ± 0.06 for wet and 0.41 ± 0.02 for dry specimens. The lack of difference indicates that the water content seems to have the same effect on fibril- and matrix

elastic properties. In a *long* fibered composite with inclusions of infinite length, the strain ratio is equal to 1 in all cases. The model consists only of highly elongated inclusions with an aspect ratio of $^{fa} a = l/d = 100$, therefore the strain ratio is between 0.99 and 1, revealing a discrepancy between their experimental results and the model output. However, the tested tissue consisted of fibrolamellar bone with a low mean dry Young's modulus of 13.9 ± 3.4 and may therefore not correspond well with the unidirectional fibril-array of this study. In this case, the strain ratio of the weakly aligned fibrolamellar fibril array must be somewhere in between the bounds of the axial- and transverse strain ratio of an unidirectional aligned fibril array if the phase material properties are the same. This hypothesis was tested but rejected by our model. The transverse strain ratio at the fibril-array level was calculated to be between 1.2 and 1.4 for input parameters close to the operation point. At this point, the fibrils in transverse direction are around 4 times softer than the extra-fibrillar matrix and therefore deform at a higher magnitude (Figs. 4, 5). Gupta et al. (2006) suggested also the mechanical role of a soft extra-collagenous interface between mineralized fibrils, allowing a substantial relative elastic displacement. This could be interpreted as an extra-fibrillar matrix with low mineral content in our model. By radically reducing the extra-fibrillar mineral content and therefore raising the elastic contrast between inclusion and matrix, the experimental axial strain ratio of 0.41 can be reached. However, this leads to unrealistically low transverse and shear stiffnesses

of the fibril-array and raises an incompatibility between our model and this suggestion.

It is important to state clearly that the presented results are predictions of a model with limitations:

First, in applying the Mori-Tanaka method on mineralized fibril, extra-fibrillar matrix and fibril-array structures, some characteristics of this tissues cannot be represented. The staggered mineral arrangement in the fibrils and their platelet-like shape is disregarded which is supposed to increase fibril stiffness (Jaeger and Fratzl 2000; Ji and Gao 2004).

Second, the real extra-fibrillar matrix is likely to be softer than predicted by the model. The mineral foam model is stiffer than the presumably real structure of mineral particles embedded in an osteopontin network.

Third, the method assumes that the modeled structures are made of constituents that satisfy the conditions of continua. Of course this is not true as the length scale of the collagen molecules have the same order of magnitude as the mineral platelets, which are regarded as inclusions in the composite model (Fig. 1). So the properties of the phases in the model are regarded as smeared over the molecular arrangement.

Four, the model assumes perfect bonding between the phases. At the nanoscale, bonding occurs on specific molecular sites (Orgel et al. 2006), which is therefore not *perfect*. In the model, the possible attenuation of the composite stiffness due to the imperfect bonding is included in the phase properties.

Five, it has to be kept in mind, that identifying the stiffness determinants of bone tissue is not sufficient. The quantities that have a low impact on stiffness in this study may be crucial for bone's strength, fracture toughness or other mechanical quantities (Ji and Gao 2004).

5 Conclusion

Using a multiscale continuum micromechanical model, we show that tissue mineralization and collagen stiffness are crucial parameters for describing fibril and fibril-array stiffness, whereas some other factors are negligible. On the other hand, we pointed out, that in using such simple micromechanical approaches, reasonable stiffness results can be easily obtained, regardless of the detailed quality of the input. Furthermore, the stepwise strain amplification mechanism in the fibril-array constituents was computed and related to experimental findings. The mineral to fibril strain ratio was well represented, while the fibril to fibril-array strain ratio will require further investigation.

Acknowledgments The authors thank the the Austrian Science Fund (FWF) for grant support (Grant No. P19009-N20), Prof. Helmut Böhm for scientific and technical support and Prof. Peter Fratzl as well as Dr. Himadri Gupta for helpful scientific discussions.

References

- Akiva U, Wagner H, Weiner S (1998) Modelling the three-dimensional elastic constants of parallel-fibred and lamellar bone. *J Mater Sci* 33(6):1497–1509
- Akkus O (2005) Elastic deformation of mineralized collagen fibrils: an equivalent inclusion based composite model. *J Biomech Eng* 127(3):383–390
- Benveniste Y (1987) A new approach to the application of mori-tanaka's theory in composite materials. *Mech Mater* 6:147–157
- Birk D, Zycband E, Woodruff S, Winkelmann D, Trelstad R (1997) Collagen fibrillogenesis in situ: fibril segments become long fibrils as the developing tendon matures. *Dev Dyn* 208(3):291–298
- Cribb A, Scott J (1995) Tendon response to tensile stress: an ultra-structural investigation of collagen:proteoglycan interactions in stressed tendon. *J Anat* 187(Pt.2):423–428
- Currey J (1969) The mechanical consequences of variation in the mineral content of bone. *J Biomech* 2(1):1–11
- Currey J (2004) Tensile yield in compact bone is determined by strain, post-yield behaviour by mineral content. *J Biomech* 37(4):549–556
- Cusack S, Miller A (1979) Determination of the elastic constants of collagen by brillouin light scattering. *J Mol Biol* 135(1):39–51
- Ebenstein D, Pruitt L (2006) Nanoindentation of biological materials. *Nano Today* 1(3):26–33
- Eppell S, Tong W, Katz J, Kuhn L, Glimcher M (2001) Shape and size of isolated bone mineralites measured using atomic force microscopy. *J Orthop Res* 19(6):1027–1034
- Eshelby J (1957) The determination of the elastic field of an ellipsoidal inclusion, and related problems. *Proc R Soc Lond A Math Phys Sci* 241(1226):376–396
- Fantner G, Adams J, Turner P, Thurner P, Fisher L, Hansma P (2007) Nanoscale ion mediated networks in bone: osteopontin can repeatedly dissipate large amounts of energy. *Nano Lett* 7(8):2491–2498
- Fratzl P, Weinkamer R (2007) Nature's hierarchical materials. *Prog Mater Sci* 52(8):1263–1334
- Fratzl P, Gupta H, Paschalis E, Roschger P (2004) Structure and mechanical quality of the collagen-mineral nano-composite in bone. *J Mater Chem* 14:2115–2123
- Fritsch A, Hellmich C (2007) 'Universal' microstructural patterns in cortical and trabecular, extracellular and extravascular bone materials: micromechanics-based prediction of anisotropic elasticity. *J Theor Biol* 244(4):597–620
- Fritsch A, Hellmich C, Dormieux L (2009) Ductile sliding between mineral crystals followed by rupture of collagen crosslinks: experimentally supported micromechanical explanation of bone strength. *J Theor Biol* 260(2):230–252
- Giraud-Guille M (1988) Twisted plywood architecture of collagen fibrils in human compact bone osteons. *Calcif Tissue Int* 42(3):167–180
- Gupta H, Wagermaier W, Zickler G, Raz-BenAroush D, Funari S, Roschger P, Wagner H, Fratzl P (2005) Nanoscale deformation mechanisms in bone. *Nano Lett* 5(10):2108–2111
- Gupta H, Seto J, Wagermaier W, Zaslansky P, Boesecke P, Fratzl P (2006) Cooperative deformation of mineral and collagen in bone at the nanoscale. *Proc Natl Acad Sci USA* 103(47):17,741–17,746
- Hansma PK, Fantner GE, Kindt JH, Thurner PJ, Schitter G, Turner PJ, Udwin SF, Finch MM (2005) Sacrificial bonds in the interfibrillar matrix of bone. *J Musculoskelet Neuronal Interact* 5(4):313–315
- Hellmich C, Ulm F (2002) Micromechanical model for ultrastructural stiffness of mineralized tissues. *J Engng Mech* 128(8):898–908
- Hellmich C, Barthlmy J, Dormieux L (2004) Mineral-collagen interactions in elasticity of bone ultrastructure—a continuum micromechanics approach. *Eur J Mech A/Solids* 23(5):783–810

- Hengsberger S, Kulik A, Zysset P (2002) Nanoindentation discriminates the elastic properties of individual human bone lamellae under dry and physiological conditions. *Bone* 30(1):178–184
- Hengsberger S, Enstroem J, Peyrin F, Zysset P (2003) How is the indentation modulus of bone tissue related to its macroscopic elastic response? a validation study. *Journal of Biomechanics* 36(10):1503–1509
- Hofmann T, Heyroth F, Meinhard H, Frnzal W, Raum K (2006) Assessment of composition and anisotropic elastic properties of secondary osteon lamellae. *J Biomech* 39(12):2282–2294
- Jaeger I, Fratzl P (2000) Mineralized collagen fibrils: a mechanical model with a staggered arrangement of mineral particles. *Biophys J* 79(4):1737–1746
- Ji B, Gao H (2004) Mechanical properties of nanostructure of biological materials. *J Mech Phys Solids* 52(9):1963–1990
- Katz JL, Meunier A (1993) Scanning acoustic microscope studies of the elastic properties of osteons and osteon lamellae. *J Biomech Eng* 115(4B):543–548
- Kotha SP, Kotha S, Guzelsu N (2000) A shear-lag model to account for interaction effects between inclusions in composites reinforced with rectangular platelets. *Compos Sci Technol* 60(11):2147–2158
- Landis W, Silver F (2002) The structure and function of normally mineralizing avian tendons. *Comp Biochem Physiol A Mol Integr Physiol* 133(4):1135–1157
- Lees S (1979) A model for the distribution of hap crystallites in bonean hypothesis. *Calcif Tissue Int* 27(1):53–56
- Lees S (1987) Considerations regarding the structure of the mammalian mineralized osteoid from viewpoint of the generalized packing model. *Connect Tissue Res* 16(4):281–303
- Lees S, Probst KS, Ingle VK, Kjoller K (1994) The loci of mineral in turkey leg tendon as seen by atomic force microscope and electron microscopy. *Calcif Tissue Int* 55(3):180–189
- Mori T (1973) Average stress in matrix and average elastic energy of materials with misfitting inclusions. *Acta Met* 21(5):571–574
- Nikolov S, Raabe D (2008) Hierarchical modeling of the elastic properties of bone at submicron scales: the role of extrafibrillar mineralization. *Biophys J* 94(11):4220–4232
- Orgel J, Irving T, Miller A, Wess T (2006) Microfibrillar structure of type I collagen in situ. *Proc Natl Acad Sci U S A* 103(24):9001–9005
- Probst KS, Lees S (1996) Visualization of crystal-matrix structure. In situ demineralization of mineralized turkey leg tendon and bone. *Calcif Tissue Int* 59(6):474–479
- Raspanti M, Congiu T, Guizzardi S (2002) Structural aspects of the extracellular matrix of the tendon : an atomic force and scanning electron microscopy study. *Arch Histol Cytol* 65(1):37–43
- Rho J, Kuhn-Spearing L, Zioupos P (1998) Mechanical properties and the hierarchical structure of bone. *Med Eng Phys* 20(2):92–102
- Rho JY, Tsui TY, Pharr GM (1997) Elastic properties of human cortical and trabecular lamellar bone measured by nanoindentation. *Biomaterials* 18(20):1325–1330
- Rijt Jvan der , Werf Kvan der , Bennink M, Dijkstra P, Feijen J (2006) Micromechanical testing of individual collagen fibrils. *Macromol Biosci* 6(9):697–702
- Roessle R (1927) Untersuchungen ueber knochenhaerte. *Beitr Pathol Anat* 77:174–208
- Sasaki N, Odajima S (1996) Elongation mechanism of collagen fibrils and force-strain relations of tendon at each level of structural hierarchy. *J Biomech* 29(9):1131–1136
- Sasaki N, Tagami A, Goto T, Taniguchi M, Nakata M, Hikichi K (2002) Atomic force microscopic studies on the structure of bovine femoral cortical bone at the collagen fibril-mineral level. *J Mater Sci Mater Med* 13(3):333–337
- Silver F, Freeman J, Seehra G (2003) Collagen self-assembly and the development of tendon mechanical properties. *J Biomech* 36(10):1529–1553
- Su X, Sun K, Cui FZ, Landis WJ (2003) Organization of apatite crystals in human woven bone. *Bone* 32(2):150–162
- Swadener J, Pharr G (2001) Indentation of elastically anisotropic half-spaces by cones and parabolae of revolution. *Philos Mag A* 81(20):447–466
- Tandon GP, Weng GJ (1984) The effect of aspect ratio of inclusions on the elastic properties of unidirectionally aligned composites. *Pol Compos* 5(4):327–333
- Wagermaier W, Gupta HS, Gourrier A, Burghammer M, Roschger P, Fratzl P (2006) Spiral twisting of fiber orientation inside bone lamellae. *Biointerphases* 1(1):1–5
- Weiner S, Traub W (1992) Bone structure: from angstroms to microns. *FASEB J* 6(3):879–885
- Weiner S, Wagner H (1998) The material bone: structure-mechanical function relations. *Annu Rev Mater Sci* 28(1):271–298
- Weiner S, Arad T, Sabanay I, Traub W (1997) Rotated plywood structure of primary lamellar bone in the rat: orientations of the collagen fibril arrays. *Bone* 20(6):509–514
- Weiner S, Traub W, Wagner H (1999) Lamellar bone: structure-function relations. *J Struct Biol* 126(3):241–255
- Withers PJ (1989) The determination of the elastic field of an ellipsoidal inclusion in a transversely isotropic medium, and its relevance to composite materials. *Philos Mag A* 59(4):759–781
- Yao H, Ouyang L, Ching W (2007) Ab initio calculation of elastic constants of ceramic crystals. *J Am Ceram Soc* 90(10):3194–3204
- Yoon Y, Cowin S (2008) The estimated elastic constants for a single bone osteonal lamella. *Biomech Model Mechanobiol* 7(1):1–11
- Zysset P, Guo X, Hoffer C, Moore K, Goldstein S (1999) Elastic modulus and hardness of cortical and trabecular bone lamellae measured by nanoindentation in the human femur. *J Biomech* 32(10):1005–1012